frontiers | Frontiers in Environmental Science

TYPE Original Research
PUBLISHED 18 October 2023
DOI 10.3389/fenvs.2023.1275087

OPEN ACCESS

EDITED BY
Xiaoyuan Zheng,
University of Shanghai for Science and Technology, China

REVIEWED BY
Claudia Prestigiacomo,
University of Palermo, Italy
Jiaqin Deng,
Central South University Forestry and Technology, China

*CORRESPONDENCE
Yingxin Zhao,
yingxinzhao@tju.edu.cn

RECEIVED 09 August 2023
ACCEPTED 22 September 2023
PUBLISHED 18 October 2023

CITATION
Qiu X, Zhao Y, Zhao C, Jin R, Li C and Mutabazi E (2023), Physicochemical and adsorptive properties of biochar derived from municipal sludge: sulfamethoxazole adsorption and underlying mechanism. *Front. Environ. Sci.* 11:1275087. doi: 10.3389/fenvs.2023.1275087

Physicochemical and adsorptive properties of biochar derived from municipal sludge: sulfamethoxazole adsorption and underlying mechanism

Xiaojie Qiu, Yingxin Zhao*, Cailian Zhao, Ruotong Jin, Chenxi Li and Emmanuel Mutabazi

School of Environmental Science and Engineering, Tianjin University, Tianjin, China

Municipal sludge waste could be transformed into useful biochar through pyrolysis process. In this study, municipal sludge-derived biochar (SBC) was successfully synthesized via the one-pot pyrolysis method, and the yield of sludge biochar gradually decreased with the pyrolysis temperature increased from 300°C to 800°C. The sludge biochar exhibited an alkaline surface due to the gradual accumulation of ash and the formation of carbonate and organic anion during high-temperature pyrolysis process. Moreover, the prepared samples were analyzed by different characterization techniques including BET, SEM, and XPS. Adsorption experiments using the optimized biochar sample of SBC800 resulted in a 95% sulfamethoxazole (SMX) removal efficiency and the maximum adsorption capacity of 7033.4 mg/kg, which was 47.5 times higher than that of SBC300. The adsorption process of SBC800 for SMX was more in line with the Freundlich and D-A isotherm model, the whole process was an exothermic reaction. SBC800 could effectively remove SMX through pore filling effect, electrostatic attraction, hydrogen bonding, hydrophobic effect, and π-π EDA interaction. Site energy distribution analysis showed that SMX preferentially occupied the high-energy adsorption site of SBC800, and then gradually diffused to the low-energy adsorption site. This study proposed a sustainable method for recycling municipal sludge for organic pollutant removal.

KEYWORDS

sludge, biochar, sulfamethoxazole, site energy distribution, adsorption

Highlight

The sludge-derived biochar was fabricated by the one-pot pyrolysis method for SMX removal.
The preparation conditions of sludge biochar were optimized.
The removal of SMX reached 95% with an adsorbent dosage of 1 g/L.
The adsorption sites on sludge biochar were analyzed by site energy distribution theory.

1 Introduction

Pharmaceuticals and personal care products (PPCPs) are widely used and continuously released to the environment from their manufacture, transportation, and disposal (Gadipelly et al., 2014). Although there was a relatively low concentration of PPCPs detected in the environment, these substances could accumulate in aquatic systems and cause adverse ecological impacts (Jin et al., 2018). Sulfonamides including sulfamethoxazole (SMX) are some of the most widely used antibiotics due to their low cost and high antimicrobial properties. The discharge of effluents from the wastewater treatment plant and aquaculture wastewater has unavoidably led to considerable exposure of SMX to the water environment (Joss et al., 2005). Without proper treatment, the discharge of SMX-contaminated wastewater into the natural environment could induce toxic effects in fish and other aquatic organisms. It was reported that residual SMX concentrations of 24.9–76.7 ng/L could be observed in the river (Gopal et al., 2021). Given the low adsorptive fate of SMX in aquatic systems, they exhibited potential hazards to animals and humans via the exposure of food and drinking water (Lai et al., 2018). There has been increasing public concern and attention about the removal of emerging contaminants (Zhang et al., 2022). Therefore, it is crucial to develop effective technologies for removing SMX and similar compounds from surface water.

Many categories of techniques were developed for SMX removal, including microbial and physicochemical processes such as electrolysis (Liu et al., 2022), Fenton (Zeng and Kan, 2022), photocatalysis (Nasuhoglu et al., 2011), and adsorption (Zhou et al., 2017). However, the Fenton method often produced a large amount of hazardous waste. Photocatalysis and electrolysis require additional energy input. Adsorption, as a typical physicochemical method, was considered a promising technology for effectively removing organic contaminants from wastewater due to its operational simplicity, effective efficiency, low energy input, and environmental friendliness (Heo et al., 2019). Diverse adsorbents, including activated carbon, carbon nanotube, and biochar have been applied to remove SMX from aqueous solution (Zhao et al., 2016; Rodríguez-Martínez et al., 2019). Among these, biochar generally prepared through partial or complete carbonization of naturally abundant biomass under oxygen-limited conditions, exhibited significant advantages towards adsorption and resource utilization due to its high porosity and abundant functional groups. Sludge biochar, as an effective adsorbent derived from different types of sludge waste, has been considered a low-cost option for water treatment adsorbents. For example, municipal sludge generally contains various heavy metal species, and other organics, which could cause severe environmental risk if they cannot be disposed of safely. Pyrolysis is generally considered a promising thermochemical process to utilize this biomass, which could produce various products including biochar, bio-oil, and biogas. Biochar, as the main product of pyrolysis, could be obtained under anaerobic or anoxic conditions (Hayes, 2006). In this way, harmful sludge waste could be transformed into biochar with abundant functional groups and active sites to achieve effective removal of organic pollutants in aqueous solution. Since the sludge biochar derived from the hazardous waste, they are inexpensive and may not require regeneration after using as adsorbent (Inyang et al., 2012). Moreover, there still needs relevant research to investigate and deliberate the application of municipal sludge derived biochar for antibiotics removal, particularly focusing on SMX. Therefore, this study aimed to bridge the knowledge gap, so that the mechanisms of sludge biochar adsorbing SMX could be well illustrated and understood.

In this study, the main objective was to understand how the physicochemical properties of biochar arising from variations in pyrolysis temperature affected the adsorption performance of SMX, and elaborate the possible mechanism of effective removal of SMX. The morphology and structural properties of the raw sludge and the prepared biochar were characterized by Brunauer Emmett and Teller (BET) surface area analysis, scanning electron microscopy (SEM), and X-ray photoelectron spectroscopy (XPS). The influence of various operational parameters on the adsorption of SMX was systematically investigated. Moreover, adsorption isotherms and kinetics analysis were also used to obtain a deep understanding of SMX removal and possible adsorption mechanisms. Finally, the different types of adsorption sites on the prepared sludge biochar were further analyzed using site energy distribution theory. This study will provide a reference for the further application of sludge biochar in antibiotics removal.

2 Materials and methods

2.1 Materials

Sulfamethoxazole (SMX; 98%), sodium hydroxide, and hydrochloric acid were all purchased through Macklin Biochemical Co. Ltd. (Shanghai, China). Acetonitrile (C_2H_3N; HPLC grade) was obtained from ANPEL Co. Ltd. All chemicals used in the study were of analytical grade and were used as received without any further processing.

2.2 Sludge biochar preparation

In the preprocessing phase, municipal sludge obtained from the sewage plant was dried at 105°C and then crushed to less than 75 μm with a mechanical mill. Afterward, the dried sludge powder was loaded into the quartz tube and put inside a tubular furnace. The pyrolysis process was calcinated at a heating rate of 10°C min^{-1} under constant nitrogen of 0.5 L min^{-1} with calcination temperatures of 300, 600, and 800°C. The resulting biochar was designated by calcination temperatures such as SBC300, SBC600, and SBC800. Moreover, the raw sludge powder was named RS.

2.3 Biochar characterization

The surface morphology and structure of the adsorbent were observed by field emission scanning electron microscope (SEM, Hitachi SU8020, Japan). The surface functional groups were identified by Fourier transform infrared spectroscopy (FTIR, Nicolet IS 10, United States). The surface charge changes of the samples were measured by a Zeta potentiometer (Zetasizer Nano ZS90, United Kingdom). The surface elemental composition and

chemical states of the adsorbents were measured by X-ray photoelectron spectroscopy (XPS, Thermo escalab 250Xi, United States). Thermal stability analysis of sludge biochar was done under air atmosphere using a STA 449 F5/F3 Jupiter thermogravimetric analyzer (TGA) between 25°C and 800°C.

2.4 Adsorption experiments and analysis method

Batch experiments were carried out in a 100 mL conical flask containing a 50 mL solution of 10 mg/L SMX, and then 1 g/L biochar sample was added into the solution to initiate the adsorption experiment. The adsorption experiment proceeded in a constant temperature oscillation chamber at 303.15 K and 160 rpm for 24 h. At each sampling occasion, a 2 mL sample was withdrawn and filtered through a 0.22 μm syringe filter for further analysis. Adsorption capacity was calculated using Eq. 1. Each experiment was repeated and average values with error bars were conducted. The reaction time was controlled within 24 h to explore the adsorption kinetics. For isotherm experiments, the initial concentration of SMX ranged from 0 to 90 mg/L, and the reaction temperatures were 293.15, 303.15, and 313.15 K. The adsorption experiments were performed at a pH of 7.0 adjusting with 1 M NaOH and HCl solutions. Ultra-high performance liquid chromatography (UPLC, Waters) equipped with a UV-Vis spectrometer and a C18 column (5 μm, 4.6 mm × 150 mm) were employed to evaluate SMX concentration at 280 nm with a mobile phase of 0.1% formic acid and acetonitrile (65:35, v: v) at a constant flow rate of 0.25 mL/min^{-1} and a 10 μL injection volume. The column temperature is 35°C.

$$q_e = \frac{(C_0 - C_e)V}{m} \tag{1}$$

2.5 Adsorption model

The pseudo-first-order kinetic model (Eq. 2), pseudo-second-order kinetic model (Eq 3), and intra-particle diffusion model (Eq. 4) were used to fit the experimental data, and the calculation formula was as follows (Gadipelly et al., 2014):

$$q_t = q_e[1 - \exp(-k1)] \tag{2}$$

$$\frac{t}{q_t} = \frac{1}{k_2 q_e^2} + \frac{t}{q_e} \tag{3}$$

$$q_t = k_i t^{0.5} + C \tag{4}$$

where t is adsorption reaction time (min); q_e and q_t are adsorption equilibrium and adsorption capacity (mg/kg) of SMX at time t. C represents the thickness of the boundary layer, the C value, the greater the show that the greater the influence of the boundary layer on the rate (Jin et al., 2018). k_1 (min^{-1}), k_2[kg/(mg·min)], and k_i [mg/kg·min$^{0.5}$] are the rate constants for pseudo-first-order kinetics model, pseudo-second-order model, and intra-particle diffusion model.

Langmuir (Eq. 5), Freundlich (Eq. 6), and Dubinin-Ashtakhov (D-A) isotherm models (Eq. 7) were used to fit the experimental data of SMX adsorption on sludge biochar (Joss et al., 2005).

Langmuir and Freundlich isotherm model:

$$q_e = \frac{q_m K_L C_e}{1 + K_L C_e} \tag{5}$$

$$q_e = K_F C_e^{1/n} \tag{6}$$

Where q_e is the equilibrium adsorption capacity of SMX on the adsorbent (mg/kg); q_m is the theoretical maximum adsorption capacity fitted by the model (mg/kg); C_e is the concentration of SMX at the adsorption equilibrium (mg/L); K_L (L/mg) and K_F [(mg/kg)/(mg/L)$^{1/n}$] are the Langmuir and Freundlich constants, respectively; K_F is related to adsorption strength, and n can represent the size of adsorption driving for Ce.

D-A isotherm model:

$$\log q_e = \log q_m - \left(\frac{\varepsilon_{SW}}{E_d}\right)^b \tag{7}$$

$$\varepsilon_{SW} = RT \ln\left(\frac{c_s}{c_e}\right) \tag{8}$$

Where ε_{SW} is the effective adsorption potential on the solid surface (J/mol); E_d is the correlation factor of the D-A model (J/mol); b is the fitting parameter of the D-A model; c_s is the solubility of SMX.

3 Result and discussion

3.1 Optimal synthesis of sludge biochar

To obtain an effective biochar adsorbent, the biochar preparation conditions were optimized in terms of yield, surface property, and ash content of sludge biochar. Figure 1A shows the yield variation of sludge biochar at different pyrolysis temperatures. With increasing the pyrolysis temperature from 300°C to 800°C, the yield of sludge biochar gradually decreased from 76.91% to 53.90%, which could be attributed to the violent decomposition of organic content in sludge at high temperatures (Yuan et al., 2015). It can be seen that the pH value of the prepared sludge biochar exhibited a trend of rising and then decreasing with the increase of pyrolysis temperature (Figure 1B). The sludge biochar SBC300 obtained by low-temperature pyrolysis was a neutral material (pH = 7.05), while the biochar prepared at 600°C reached the maximum pH value of 10.04. This difference could be ascribed to the incomplete decomposition of organic matter under low pyrolysis temperatures, resulting in the abundant acidic oxygen-containing functional groups on the surface of sludge biochar. However, when the pyrolysis temperature was further increased, the organic acids on the biochar surface would gradually decompose to form carbonates, which was the main source of the alkaline component of biochar under high-temperature pyrolysis (Yuan et al., 2011). Besides, carbonyl groups and hydroxyl groups could exist in the form of organic anions on the surface of sludge biochar and then combined with H^+ to induce the alkaline surface of the material (Chen et al., 2011). Furthermore, the pH value of the biochar surface decreased when the pyrolysis temperature was greater than 600°C, which could be attributed to the thermal decomposition of alkali salts consisting of Ca, Mg, K, etc. In addition, the ash content of samples increased with increasing pyrolysis temperature from 300°C to 800°C

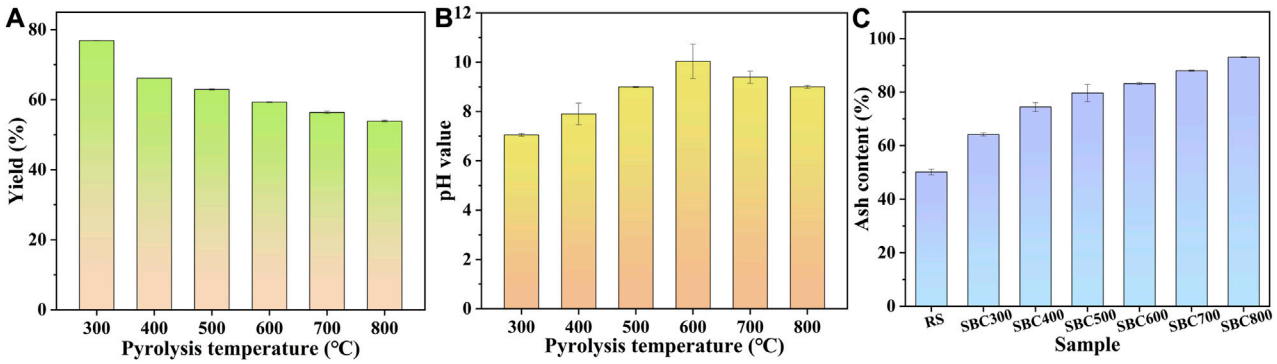

FIGURE 1
Pyrolysis properties of sludge biochar: **(A)** yield; **(B)** pH value and **(C)** ash content of the sludge biochar at different pyrolysis temperatures.

(Figure 1C), indicating that the inorganic components (such as Si and Ca) produced by sludge pyrolysis are gradually enriched.

3.2 Characterization of biochar

In order to observe the surface structure of sludge biochar at different pyrolysis temperatures, the adsorbent was morphologically characterized by FESEM (Figures 2A–D; Supplementary Figure S1). It was observed that the raw dewatered sludge exhibited an irregular block structure and relatively flat surface. However, the surface of sludge biochar became rough with increasing pyrolysis temperature (Supplementary Table S1), indicating its gradually developed pore structure. It was worthing that a large amount of porous structure and trench structure could be observed in the SBC800 sample, suggesting that the higher pyrolysis temperature was conducive to the formation of abundant porous structure on the surface of sludge biochar. Hence, the obtained biochar exhibited a large specific surface area, which could provide more active adsorption sites for the adsorption and removal of organic pollutants. TG and DTG curves exhibited three stages during the pyrolysis process of dewatered sludge (Figure 2E). In the first stage, a slight mass loss of 2.5% could be observed below 110 °C, which can be attributed to the evaporation of free and bound water in the sludge. The main weight loss occurred in the second stage, and 35.4% of components were lost within the temperature range of 110°C–540°C. It has been reported that the volatile aliphatic organic matter, cellulose, protein, and other organics in the sludge would be decomposed in this temperature range (Shu-Rong et al., 2006). The third stage is the decomposition of difficult volatile organic compounds and the volatilization of a few inorganic substances. This stage showed a weight loss of only 6.6% corresponding to a temperature of 540°C–800°C. Ultimately, the residual sample mainly existed in the form of ash and carbon. Moreover, the DSC test displayed the dynamic change of the pyrolysis process. As shown in Figure 2F, the endothermic reaction occurred at temperatures ranging from room temperature to 156°C, which corresponded to the volatile endothermic phase of water in the DTG curve. The overall manifestation of the 156°C–485°C stage displayed an exothermic reaction because the anaerobic pyrolysis of organic matter including aliphatic and carbohydrates into aromatic compounds could release a lot of heat (Mimmo et al., 2014). Later, the whole system gradually turned into an endothermic state with the decomposition of volatile organic compounds.

XPS analysis was further used to investigate the chemical composition of the prepared biochar. As shown in Table 1, the relative content of C, H, N, and O in biochar decreased by 6.29%, 2.04%, 2.73%, and 7.60% to the increase of pyrolysis temperature from 300°C to 800°C, which was attributed to the fact that the organics (such as fatty, sugars, and proteins) in dehydrated sludge could be pyrolyzed and further convert into hydrocarbons during the pyrolysis process. Generally, the ratio of H to C can be used to represent the aromaticity and hydrophobicity of the prepared material, and the lower ratio of H/C meant the greater aromaticity and hydrophobicity of the material (Yuan et al., 2013). As shown in Table 1, the ratio of H/C of the prepared biochar decreased with the increase of the pyrolysis temperature, indicating that unsaturated carbon would gradually transform into relatively stable aromatic carbon during the pyrolysis and carbonization process of dehydrated sludge. Therefore, SBC800 exhibited the highest hydrophobicity, which was agreed with the research results of Wu et al. (Wu et al., 2022).

3.3 Adsorption performance on SMX removal

Figure 3A shows the adsorption capacity of SMX by prepared sludge biochar at different pyrolysis temperatures. As shown, the adsorption capacity of SBC800 could reach 7,033.4 mg/kg, which was significantly higher than that of the prepared samples at other pyrolysis temperatures. It should be noted that the adsorption capacity of SBC800 was increased by 47.5 times compared with SBC300 (147.96 mg/kg). It was speculated that the larger specific surface area, stronger hydrophobic surface, and higher degree of aromatization of the prepared biochar contributed to the high adsorption affinity of SBC800 for SMX. Combined with the adsorption performance and the physicochemical properties of sludge biochar, SBC800 was selected as a typical biochar for a follow-up study.

The dosage of adsorbent was an important parameter to investigate the adsorption performance of sludge biochar. The

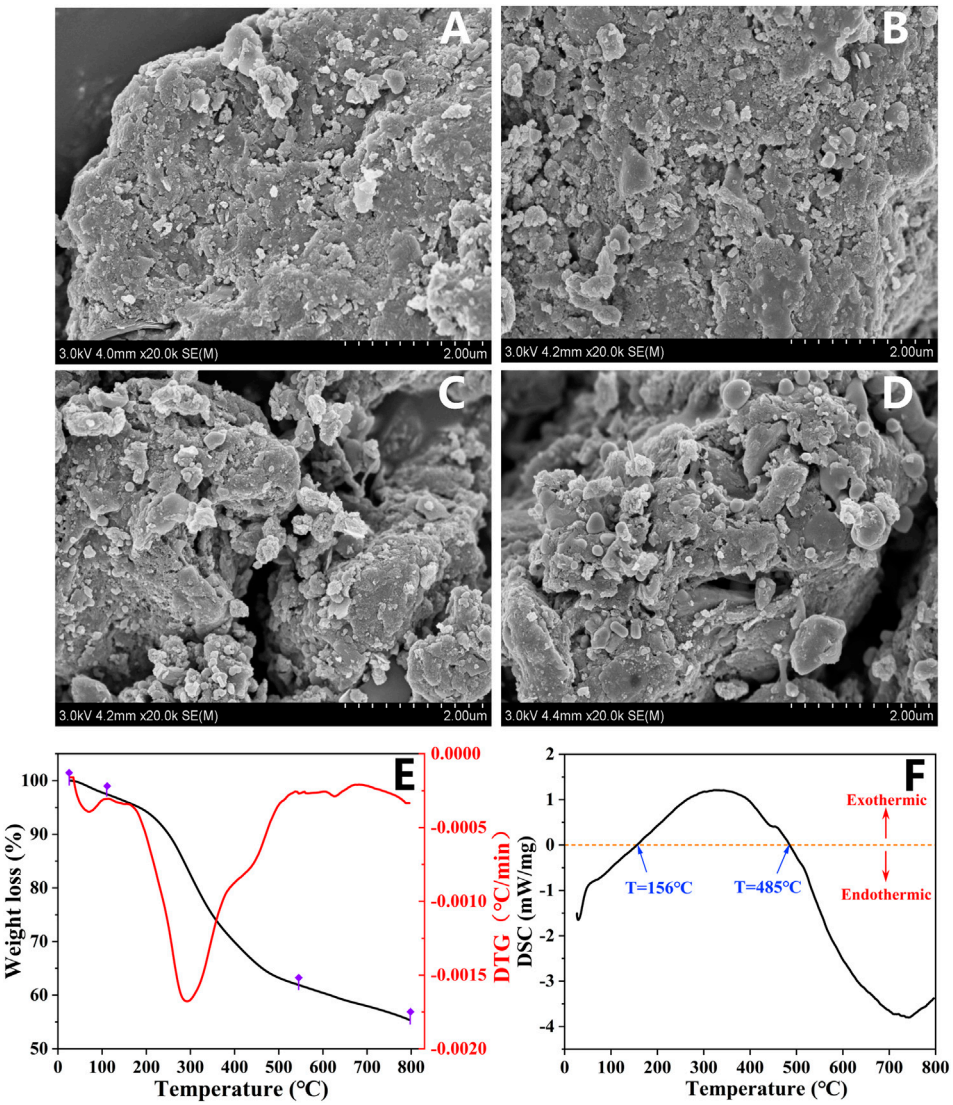

FIGURE 2
Characteristics: FESEM image of the prepared **(A)** RS, **(B)** SBC300, **(C)** SBC600, **(D)** SBC800; **(E)** pyrolysis steps obtained from thermogravimetric analysis; **(F)** DSC curve of dewatered sludge obtained from the pyrolysis process.

TABLE 1 The elemental composition of the prepared sludge biochar.

Sample	Element content					H/C
	C (%)	H (%)	N (%)	S (%)	O (%)	
SBC300	20.80	2.55	3.47	0.9	17.10	0.123
SBC600	17.77	0.74	1.9	1.31	13.32	0.042
SBC800	14.51	0.51	0.7	1.35	9.50	0.035

experimental result is shown in Figure 3B. The adsorption capacity of SBC800 for SMX first increased and then decreased with an increase in the dosage of SBC800, suggesting that increasing the dosage of the adsorbent within a certain range could effectively increase the adsorption capacity for pollutants. However, the excessive dosage of adsorbent could overlap the adsorption sites and reduce effective active sites available for SMX, resulting in decreased adsorption performance (Wang et al., 2010). Moreover, there also some studies that showed that the decrease in unit adsorption capacity may be due to the concentration gradient between the adsorbent and the adsorbate decreasing with the increase of the adsorbent dosage, rendering a limited contaminant diffusion rate (Liu et al., 2021). In general, increasing the dosage of SBC800 could efficaciously improve the adsorption capacity of SMX, but excessive adsorbent dosage could lead to the waste of adsorbent and increase the disposal cost during the adsorption process, therefore, 1.0 g/L was selected as the optimal dosage for subsequent adsorption experiments. The effect of adsorption time on the adsorption performance of SMX was investigated in Figure 3C. The adsorption capacity raised sharply in the first 30 min, and could reach 93.8% of the adsorption equilibrium amount within 30 min, which was 7,482.9 mg/kg. There was a slight decrease in the amount of adsorption in the next half hour, which may result from some of the weakly adsorbed

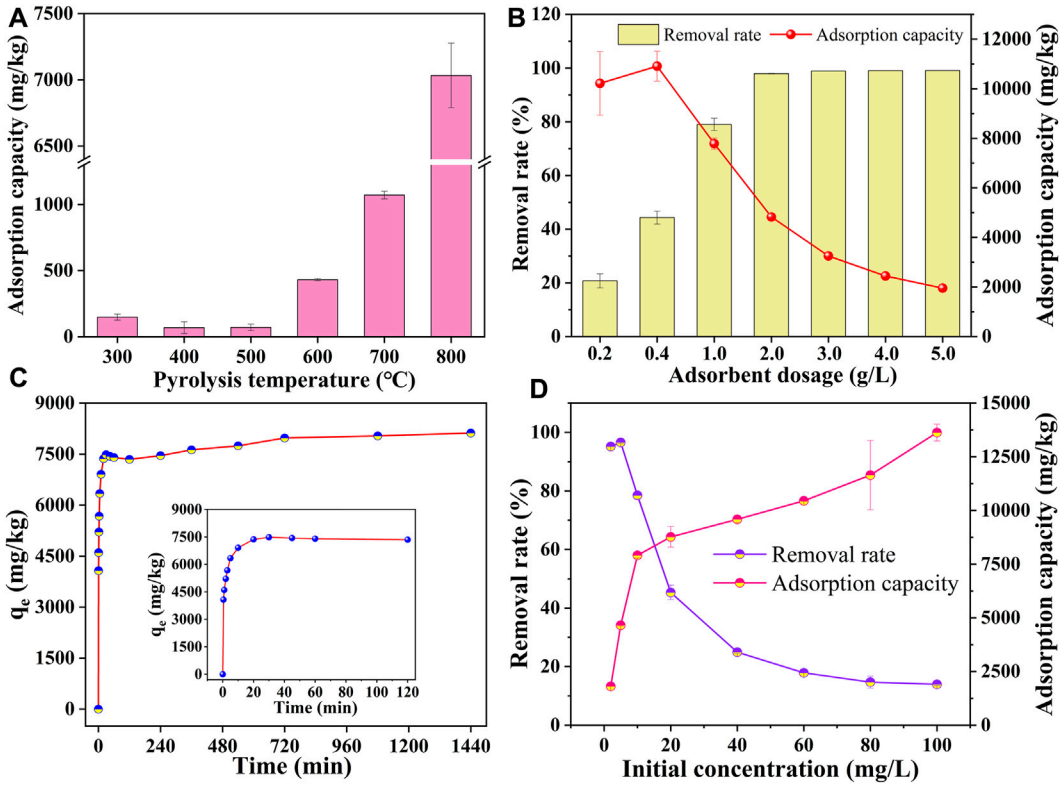

FIGURE 3
(A) Adsorption of sulfamethoxazole by sludge biochar at different pyrolysis temperatures; **(B)** effect of the SBC800 dosage ([dosage] = 0.2–5.0 g L^{-1}, [C_0] = 10 mg L^{-1}, [pH] = 7.0, [temperature] = 30°C); **(C)** effect of contact time ([dosage] = 1.0 g L^{-1}, [C_0] = 10 mg L^{-1}, [pH] = 7.0, [temperature] = 30 C); **(D)** effect of initial concentration of SMX ([dosage] = 1.0 g L^{-1}, [C_0] = 0–100 mg L^{-1}, [pH] = 7.0, [temperature] = 30°C).

SMX desorbed from the surface of SBC800 under the vibration of the shaking table. As shown in Figure 3C, the adsorption amount increased slowly and gradually tended to equilibrium, and reached the adsorption equilibrium at 12 h. This phenomenon indicated that the adsorption sites on the surface and porous structure of SBC800 were sufficient in the early stage of adsorption, and the large concentration difference between the solid-liquid phases increased the mass transfer driving force (Tran et al., 2017) so that SMX could quickly occupy the adsorbed sites. However, a large number of sites on the surface of SBC800 was exploited as extended over time, the declined driving force resulted in the decreased adsorption rate and the adsorption capacity tended to equilibrium. In addition, it has been reported that the effect of electrostatic repulsion between SMX molecules in the later adsorption stage was also one of the reasons for the slowed diffusion rate of the adsorbate into the adsorbent (XIONG et al., 2010). The influence of the initial concentration of SMX ranging from 2 to 100 mg/L on the adsorption performance of SBC800 was displayed in Figure 3D. The removal rate of SMX decreased from 95.18% to 13.94% with increasing initial concentration from 10 to 100 mg/L. The equilibrium capacity increased from 1806.18 mg/kg to 13627.68 mg/kg with the increase of the initial concentration in the range of 2–80 mg/L. According to previous studies, the initial concentration could affect the driving force of molecular diffusion by changing the concentration gradient between biochar and solution, thereby affecting the removal effect of biochar on pollutants. Therefore, there were relatively more active adsorption sites and functional groups on the surface of sludge biochar at the low initial concentration of SMX, so that SMX could be rapidly adsorbed and the high removal rate was obtained. However, the adsorbent surface was far from saturated because of the limited amount of SMX, thus, resulting in lower adsorption capacity. With the increase of the initial concentration of SMX, the concentration difference between the solid phase and the liquid phase and driving force distinctly increased, and the effective collision between SMX and the adsorption site was greatly improved, resulting in a significant increase in the adsorption capacity. However, it should be pointed that the number of active sites and functional groups of the adsorbent was limited, therefore, the removal rate decreased and the adsorption capacity gradually became saturated with the increase of initial concentration.

3.4 Adsorption models

The experimental data were fitted using pseudo-first-order kinetics, pseudo-second-order kinetics, and intra-particle diffusion models to further investigate the adsorption process and the rate-limiting step. As shown in Table 2 and Figure 4A, the correlation coefficient R^2 of the pseudo-first-order kinetic model was greater than that of the pseudo-second-order model, and the

TABLE 2 Pseudo-first-order and pseudo-second-order kinetic model fitting parameters.

Adsorbent	$q_{e,exp}$ (mg/kg)	Pseudo-first-order fitting			Pseudo-second-order fitting		
		k_1 (min^{-1})	$q_{e,cal}$ (mg/kg)	R^2	k_2 [kg/(mg·min)]	$q_{e,cal}$ (mg/kg)	R^2
SBC800	776.91	0.850	7411.26	0.899	1.281×10^{45}	6872.35	0.644

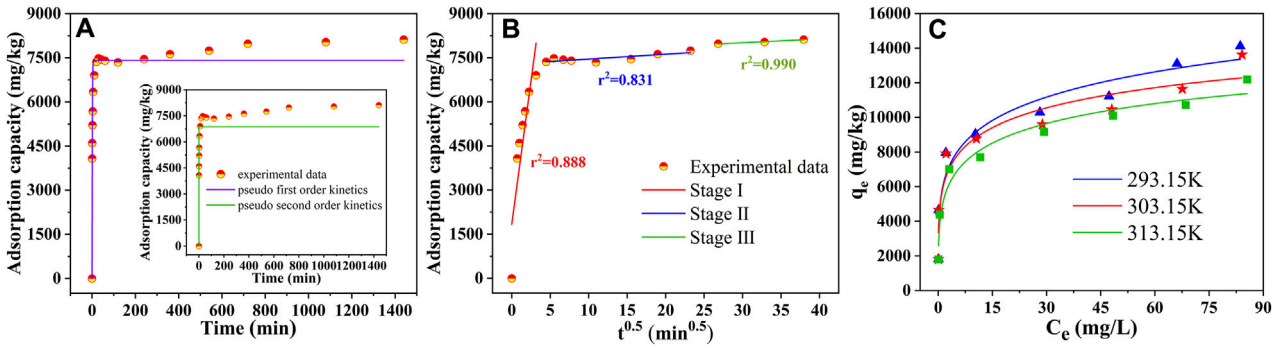

FIGURE 4
(A) The linear fittings of pseudo-first-order and pseudo-second-order fitting ([dosage] = 1.0 g L^{-1}, [C_0] = 10 mg L^{-1}, [pH] = 7.0, [temperature] = 30°C); **(B)** intraparticle diffusion model of SBC800; **(C)** D-A isotherm model fitting for SMX adsorption.

TABLE 3 Intraparticle diffusion model parameters.

Adsorbent	Stage I		Stage II		Stage III	
	K_{i1} [mg/(kg·$min^{0.5}$)]	C_1 (mg/kg)	K_{i2} [mg/(kg·$min^{0.5}$)]	C_2 (mg/kg)	K_{i3} [mg/(kg·$min^{0.5}$)]	C_3 (mg/kg)
SBC800	1950.70	1831.94	16.48	7290.97	12.81	7627.94

theoretical adsorption capacity obtained by the pseudo-first-order kinetic model was closer to the measured adsorption capacity, indicating that pseudo-first-order kinetics fitted better. It is well-known that the pseudo-first-order kinetic model assumed that the adsorption process was controlled by a diffusion step, which is dominated by physisorption. Therefore, the intraparticle diffusion model was used to further investigate the diffusion mechanism of SMX on SBC800. As displayed in Figure 4B; Table 3, the curve of adsorption capacity *versus* $t^{0.5}$ exhibited an excellent linear and passed through the origin, therefore, intraparticle diffusion was the only rate-limiting step during the adsorption process (Wang et al., 2011; Liao et al., 2012). Moreover, the curves fitted in this study were multi-linear, suggesting that the adsorption process of SMX was also affected by extra-particle diffusion processes (Liao et al., 2020; Vivas and Cho, 2021). Specifically, the adsorption of SMX by SBC800 in Figure 4B proceeded in three stages: the first stage exhibited an initially steep linearity, which represented the fast membrane diffusion. At this stage, the diffusion of SMX molecules to the outer surface of SBC800 accelerated by sufficient active sites and a high concentration difference. Stage II is the intra-particle diffusion stage, in which SMX molecules migrate to the pore structure of the adsorbent and are adsorbed on the inner surface of the material (Song et al., 2021). Besides, the low diffusion rate of k_{i2} indicated that this stage was a slow diffusion process. The third stage corresponded to the adsorption equilibrium phase of SMX with a lower diffusion rate (Yan et al., 2017). Notably, the C value was constantly increasing throughout the adsorption process, revealing the enhanced boundary layer effect. The downward trend in the k_i values in Table 3 showed that the diffusion rate is further restricted over time caused by the weakening of the driving force and the reduction of porosity (Gao and Pedersen, 2005).

The Langmuir, Freundlich, and D-A isotherm models were used to fit the process of SBC800 adsorption of SMX, and the calculated parameters were summarized in Tables 4, 5. It can be seen that the fitted correlation coefficients R^2 of the Freundlich model and the D-A model were both greater than 0.9. The Freundlich and D-A models could be more suitable for simulating the adsorption behavior of SMX on SBC800 compared with the Langmuir model. These results illustrated that the adsorption process of SMX by SBC800 was heterogeneous adsorption, and the multi-layer adsorption could be observed due to the interaction between adsorbate molecules. Moreover, the $1/n$ values at three different adsorption temperatures were all between 0 and 0.5, suggesting that the adsorption process belonged to preferential adsorption. It is noteworty that the maximum adsorption capacity of SMX obtained by the Freundlich and D-A model decreased as the temperature increased from 293.15 to 313.15 K (Figure 4C). In addition, the K_F value, which was related to the adsorption strength, decreased to

TABLE 4 Fitting results for different isotherm models.

(K)	Langmuir		Freundlich		D-A		
	q_m (mg/kg)	K_L (L/mg)	K_L [(mg/kg)/(mg/L)$^{1/n}$]	n	q_m (mg/kg)	b	Ed (J/mol)
293.15	11565.2	2.27	5663.5	5.09	16068.0	1.16	13525.5
303.15	10798.4	2.76	5531.0	5.41	14608.0	1.33	16010.2
313.15	10198.4	1.18	4732.8	4.93	13875.2	1.45	16093.0

TABLE 5 Correlation coefficients for three isotherm models.

(K)	Langmuir	Freundlich	D-A
293.15	0.835	0.944	0.944
303.15	0.835	0.916	0.918
313.15	0.868	0.962	0.966

4.93 as the adsorption temperature increased to 313.15 K, revealing that the SMX adsorption on SBC800 was an exothermic process.

3.5 Adsorption mechanism of SMX

Supplementary Table S2 exhibited the BET parameters before and after the adsorption process. The total specific surface area, micropore specific surface area, external pore specific surface area, and total pore volume all decreased after adsorption. In addition, the pore size position of SBC800 concentrated distribution decreased from 4.05 nm to 3.79 nm (Supplementary Figure S2), indicating that SMX molecules can be trapped by the adsorbent through pore filling. The linear correlation analysis was used to further demonstrate the above conclusion. As shown in Figure 5A, the linear relationship between the specific surface area, total pore volume, and SMX adsorption capacity of SBC300, SBC600, and SBC800 were analyzed. The results showed that the correlation coefficient R^2 was determined to be 0.997 and 0.993, respectively, indicating that the pore-filling effect was crucial for the adsorption of SMX on the sludge biochar (Shen et al., 2015). It should be noted that the micropore area and external surface area of SBC800 decreased by 91.40% and 2.17%, respectively. This result clearly proved that the micropore area of SBC800 was fully occupied after SMX adsorption, and the external surface area was also partially utilized. The molecular size of SMX was reported to be around 6.23–13.62 Å (Nielsen et al., 2014), which was smaller than the average pore size of the SBC800 adsorbent. Therefore, the mesoporous characteristics of the prepared SBC800 could contribute to the reduction of the size exclusion effect during the adsorption process (Liu et al., 2017), thereby facilitating the entry of SMX into the porous structure of the prepared material.

The pH value of the solution could affect the surface charge of the adsorbent and the morphology of the adsorbate, thus exhibiting an important effect on the adsorption performance of the material (Chen et al., 2019). Figure 5B showed that SMX with two pK_a values of 1.7 and 5.7 (Peiris et al., 2017), which means that sulfamethazine mainly existed in the ion form of SMX^+ and SMX^- at pH < 1.7 or pH > 5.7 due to the protonation of amino group and the deprotonation of the sulfonamide, and mainly in the form of a neutral molecule (SMX^0) at pH 1.7–5.7. Zeta potential test showed the point of zero charge (pH_{pzc}) of SBC800 was determined to be 6.71 (Figure 5C). SMX^- gradually increased when pH was greater than 3.7, therefore, the positively charged surface of SBC800 could effectively absorb SMX^- at pH 3.7–6.7 due to the electrostatic attraction force. Moreover, the high-resolution N 1s spectra obtained from XPS analysis showed that the relative content of protonated nitrogen (N^+) decreases from 80.90% to 74.11% (Figure 5E), which further implying that electrostatic attraction would be one of the important mechanisms for the SMX adsorption by SBC800 biochar (Zhang L. et al., 2020).

FTIR spectrum in Figure 5D showed that three new characteristic peaks appeared in SBC800 after SMX adsorption, among which 1,388 cm^{-1} is the symmetric peak of sulfone group (O=S=O) in SMX, 1,454 cm^{-1} can be attributed to the vibration of isoxazole in SMX, and 1,542 cm^{-1} is caused by the vibration of $-NH_2$ in the benzene or -C=N in oxazole of SMX molecules (Chamundeeswari et al., 2014; Li et al., 2019). These new absorption peaks clearly indicated the successful adsorption of SMX on SBC800. Moreover. the spectrum bands of N-H and O-H stretching vibration on the solid surface shifted from 3,435 cm^{-1} to 3,440 cm^{-1}, while the absorption peak of C-OH at 1,050 cm^{-1} shifted to 1,046 cm^{-1}, suggesting that the amino, hydroxyl, and carboxyl groups on the surface of SBC800 could form hydrogen bonding forces with $-NH_2$, and -NH- in SMX molecules (Li Z. et al., 2020; Zhang Y. et al., 2020). In addition, the carboxyl C=O absorption peak at 1,628 cm^{-1} moved to a lower wavenumber, which further proved the above conclusion. To further elucidate the adsorption mechanism of SMX on SBC800, XPS analysis was used to characterize SBC800 before and after SMX adsorption. After adsorption, the relative contents of N and S elements on SBC800 increased from 3.18% to 1.41%–3.61% and 2.18% (Supplementary Table S3), respectively, further indicating the successful adsorption of SMX. The high-resolution C1s spectra were deconvolved into five peaks (Figure 5F), where peaked at 285.48, 286.70, and 289.28 eV binding energies were attributed to C-O, C=O, and O=C-O, respectively (Li R. et al., 2020). However, the binding energy of these peaks was redshifted, indicating that oxygen-containing functional groups were involved in the adsorption process by forming hydrogen bonds (Pap et al., 2020). Furthermore, the high-resolution spectrum of O 1s was deconvolved to peaks of

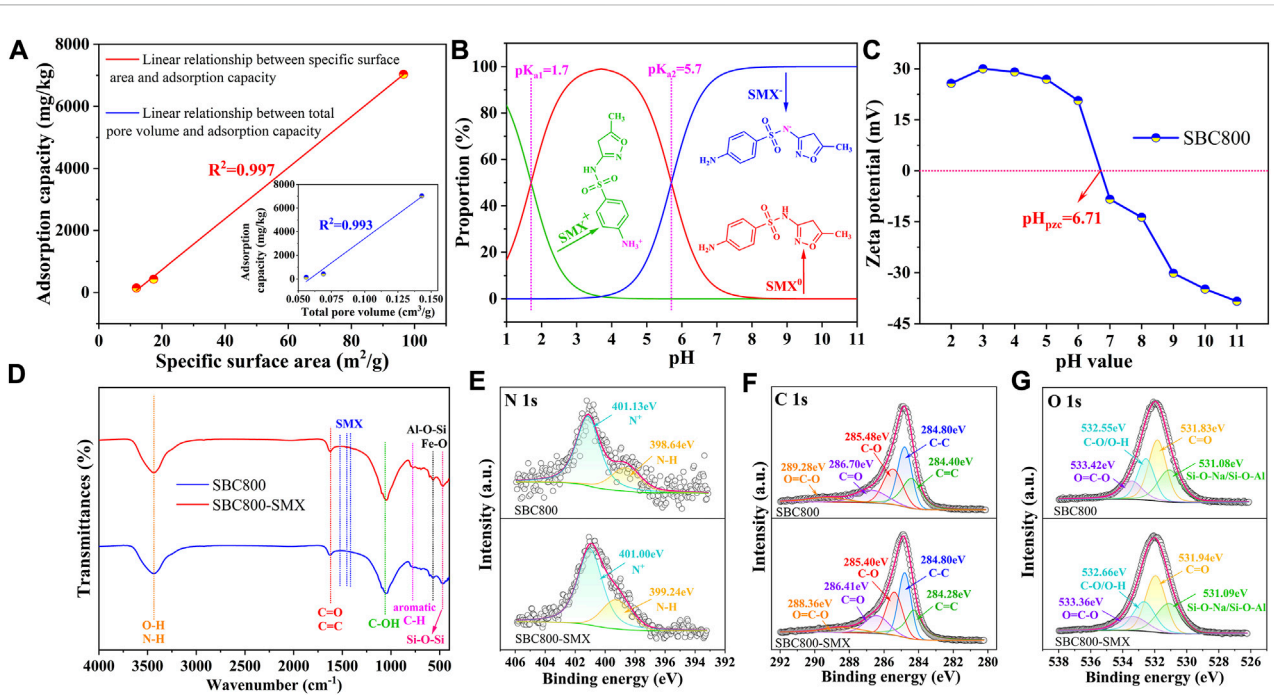

FIGURE 5
(A) Linear correlation analysis between specific surface area, total pore volume, and SMX adsorption capacity of SBC800; **(B)** Zeta potential of SBC800 obtained from Zeta analyzer; **(C)** morphological distribution of SMX at different pH values; **(D)** FTIR spectra before and after adsorption; XPS high-resolution spectrum of **(E)** N 1s, **(F)** O 1s, and **(G)** C 1s before and after SMX adsorption.

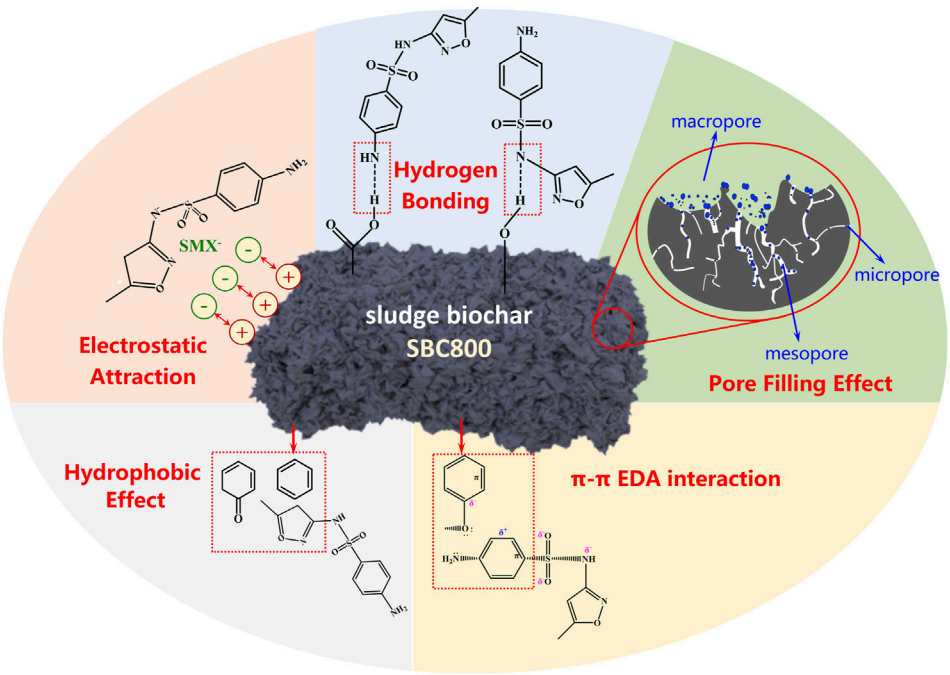

FIGURE 6
The schematic diagram of the adsorption mechanism of SBC800.

C=O, C-O/O-H, and O=C-O at binding energies 531.83, 532.55, and 533.42, respectively and then these peaks moved to the binding energy of 531.94, 532.66, and 533.36 eV after adsorption (Figure 5G). The position of the N-H peak in the N 1s high-resolution spectrum shifted from 398.64 to 399.24 eV after adsorption. These findings illustrated that hydrogen

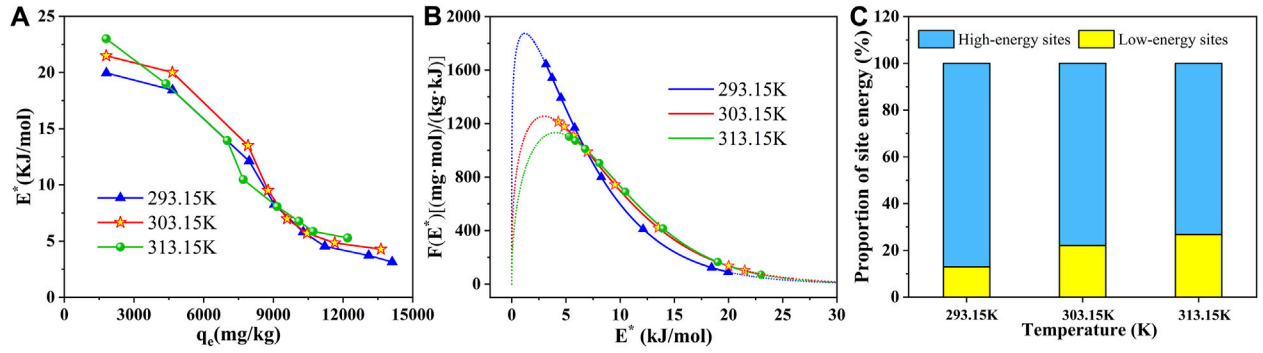

FIGURE 7
(A) The variation of site energy E* with equilibrium adsorption capacity of SBC800; **(B)** site energy distribution based on D-A isotherm model; **(C)** proportion of high and low site energy in SBC800/SMX system.

TABLE 6 The integration curve of the site energy distribution of SBC800.

	SBC800 (293.15K)	SBC800 (303.15K)	SBC800 (313.15K)
Total integral area	16018.5	14535.5	13827.8
Low-energy site area	2068.4	3208.1	3700.1
High-energy site area	13950.1	11327.4	10127.7

bonding is an important mechanism of SBC800 adsorption of SMX (Liu et al., 2020).

FTIR spectrum in Figure 5D exhibited the absorption peak (1,628 cm^{-1}) related to C=C of the benzene ring shifted to the low wavenumber after adsorbing SMX, which can be explained that the π-π electron donor and acceptor interaction (π-π EDA) was involved in the removal of SMX (Liu et al., 2019; Zhang R. et al., 2020). The redshift of aromatic C-H at the wavenumber of 778 cm^{-1} further demonstrated the engagement of *π-π* EDA effect. In addition, the C 1s spectrum of SBC800 showed that the peak at 284.40 eV belonging to sp^2 hybrid carbon (C=C) moved towards the low binding energy (284.28 eV) after adsorption, indicating that C=C bonds exhibited a potential to lose electrons and act as a π electron donor to interact with SMX (electron acceptor) for *π-π* EDA effect (Wang et al., 2015). In summary, the prepared sludge biochar could achieve effective adsorption of SMX through pore filling, electrostatic attraction, hydrogen bonding, and *π-π* EDA interaction, and the schematic diagram of the adsorption mechanism of SBC800 is shown in Figure 6.

3.6 Site energy distribution analysis

The site energy distribution theory was employed to further elaborate the adsorption behavior in the SBC800/SMX system (Text S1). Based on the above analysis, the adsorption process of SMX on the SBC800 was best fitted with a D-A isotherm model. Therefore, the change in energy distribution of adsorption sites on the surface of SBC800 was further explored based on the D-A model. Figure 7A shows the variation of the potential energy E* of SBC800 adsorbing SMX with q_e at different temperatures. It can be seen that the E* value of SBC800 decreased sharply with the increase of q_e, which indicated that SMX molecules preferentially occupied the high-energy adsorption site of SBC800 during the adsorption process, and then gradually diffused to the low-energy adsorption site (Yan and Niu, 2018). In order to explore the interface interaction between SMX and SBC800 and better reveal the adsorption mechanism, the change of frequency function F (E*) with E* was further analyzed. The experimental range of E* was calculated based on the equilibrium concentration and maximum solubility of SMX, and plotted with a solid line in Figure 7B, while the site energy curve of the rest was represented by a dashed line. It should be pointed out that the negative value of E* has no physical significance because the equilibrium concentration of SMX cannot be greater than its maximum solubility in practical application (Shen et al., 2015). The approximate site energy curve of SBC800 exhibited a clear unimodal distribution, namely, F (E*) first grew to a peak with the increase of site energy E*, and then gradually decreased to close to zero. The upward trend suggested that a small number of solute molecules were forced to occupy sites with lower energies under high SMX concentrations, whereas SMX molecules prefer to occupy high-energy sites at low concentrations (Zhang et al., 2021). However, due to the low F (E*) value, extremely high and low site energies made a negligible contribution to the maximum adsorption capacity. Theoretically, the area under the F (E*)-E* curve can be considered as the number of available adsorption sites in a specific energy range (Liu et al., 2016; Chen et al., 2017). Therefore, the curve was integrated in the range 0–30 kJ/mol of E*. As shown in Figure 7C and Table 6, SMX preferentially occupied the high-energy adsorption site, and then effectively removed through hydrogen bonding effect and *π-π* EDA interactions. In addition, the total number of available adsorption sites on SBC800 at different temperatures was ordered as 293.15 K > 303.15 K > 313.15 K,

suggesting that low temperature was more conducive to SMX adsorption, which was consistent with the isotherm fitting results.

4 Conclusion

In this study, a serious of municipal sludge-derived biochar (SBC300-800) was successfully prepared through a simple pyrolysis method for SMX adsorption and removal. The synthesis parameters were optimized systematically to achieve SMX adsorption capacity of 7033.4 mg/kg, which was 47.5 times higher than that of the prepared SBC300. Additionally, the adsorption is mainly physical adsorption, and the adsorption rate is jointly controlled by intra-particle diffusion and external diffusion. The adsorption mechanism of SMX in aqueous solution by SBC800 biochar composites included pore filling, electrostatic attraction, hydrogen bonding, and π-π EDA interaction. Therefore, the SBC800 sample obtained from the pyrolysis of sludge would be an effective and promising adsorbent for antibiotic adsorption. This research will be conductive for sludge treatment and resource utilization via the enhanced adsorption capacity for pollutant removal.

Data availability statement

The raw data supporting the conclusion of this article will be made available on request.

Author contributions

XQ: Formal Analysis, Investigation, Writing–original draft, Writing–review and editing. YZ: Funding acquisition, Supervision, Writing–review and editing. CZ: Data curation, Formal Analysis, Writing–review and editing. RJ: Investigation, Writing–review and editing. CL: Investigation, Software, Writing–review and editing. EM: Investigation, Software, Writing–review and editing.

Funding

The author(s) declare financial support was received for the research, authorship, and/or publication of this article. This work was supported by the National Natural Science Foundation of China (No. 52170046).

Conflict of interest

The authors declare that the research was conducted in the absence of any commercial or financial relationships that could be construed as a potential conflict of interest.

Publisher's note

Supplementary material

The Supplementary Material for this article can be found online at: https://www.frontiersin.org/articles/10.3389/fenvs.2023.1275087/full#supplementary-material

References

Chamundeeswari, S. P., James Jebaseelan Samuel, E., and Sundaraganesan, N. (2014). Molecular structure, vibrational spectra, NMR and UV spectral analysis of sulfamethoxazole. *Spectrochimica Acta Part A Mol. Biomol. Spectrosc.* 118, 1–10. doi:10.1016/j.saa.2013.07.063

Chen, D., Chen, C., Shen, W., Quan, H., Chen, S., Xie, S., et al. (2017). MOF-derived magnetic porous carbon-based sorbent: Synthesis, characterization, and adsorption behavior of organic micropollutants. *Adv. Powder Technol.* 28, 1769–1779. doi:10.1016/j.apt.2017.04.018

Chen, Q., Zheng, J., Xu, J., Dang, Z., and Zhang, L. (2019). Insights into sulfamethazine adsorption interfacial interaction mechanism on mesoporous cellulose biochar: Coupling DFT/FOT simulations with experiments. *Chem. Eng. J.* 356, 341–349. doi:10.1016/j.cej.2018.09.055

Chen, X., Chen, G., Chen, L., Chen, Y., Lehmann, J., Mcbride, M. B., et al. (2011). Adsorption of copper and zinc by biochars produced from pyrolysis of hardwood and corn straw in aqueous solution. *Bioresour. Technol.* 102, 8877–8884. doi:10.1016/j.biortech.2011.06.078

Gadipelly, C., Pérez-González, A., Yadav, G. D., Ortiz, I., Ibá?ez, R., Rathod, V. K., et al. (2014). Pharmaceutical Industry Wastewater: Review of the Technologies for Water Treatment and Reuse. *Industrial Eng. Chem. Res.* 53, 11571–11592. doi:10.1021/ie501210j

Gao, J., and Pedersen, J. A. (2005). Adsorption of Sulfonamide Antimicrobial Agents to Clay Minerals. *Environ. Sci. Technol.* 39, 9509–9516. doi:10.1021/es050644c

Gopal, C. M., Bhat, K., Ramaswamy, B. R., Kumar, V., Singhal, R. K., Basu, H., et al. (2021). Seasonal occurrence and risk assessment of pharmaceutical and personal care products in Bengaluru rivers and lakes, India. *J. Environ. Chem. Eng.* 9, 105610. doi:10.1016/j.jece.2021.105610

Hayes, M. H. B. (2006). Biochar and biofuels for a brighter future. *Nature* 443, 144. doi:10.1038/443144c

Heo, J., Yoon, Y., Lee, G., Kim, Y., Han, J., and Park, C. M. (2019). Enhanced adsorption of bisphenol A and sulfamethoxazole by a novel magnetic CuZnFe2O4–biochar composite. *Bioresour. Technol.* 281, 179–187. doi:10.1016/j.biortech.2019.02.091

Inyang, M., Gao, B., Yao, Y., Xue, Y., Zimmerman, A. R., Pullammanappallil, P., et al. (2012). Removal of heavy metals from aqueous solution by biochars derived from anaerobically digested biomass. *Bioresour. Technol.* 110, 50–56. doi:10.1016/j.biortech.2012.01.072

Jin, Q., Zhang, S., Wen, T., Wang, J., Gu, P., Zhao, G., et al. (2018). Simultaneous adsorption and oxidative degradation of Bisphenol A by zero-valent iron/iron carbide nanoparticles encapsulated in N-doped carbon matrix. *Environ. Pollut.* 243, 218–227. doi:10.1016/j.envpol.2018.08.061

Joss, A., Keller, E., Alder, A. C., Göbel, A., McArdell, C. S., Ternes, T., et al. (2005). Removal of pharmaceuticals and fragrances in biological wastewater treatment. *Water Res.* 39, 3139–3152. doi:10.1016/j.watres.2005.05.031

Lai, L., Peng, J., Ren, Y., Li, J., Zhang, Y., and Lai, B. (2018). Catalytic Ozonation of Succinic Acid in Aqueous Solution by Co/Al 2 O 3 -EPM: Performance, Characteristics, and Reaction Mechanism. *Environ. Eng. Sci.* 35, 1309–1321. doi:10.1089/ees.2018.0028

Li, R., Zhang, Y., Deng, H., Zhang, Z., Wang, J. J., Xiao, R., et al. (2020b). Removing tetracycline and Hg(II) with ball-milled magnetic nanobiochar and its potential on

polluted irrigation water reclamation. *J. Hazard. Mater.* 384, 121095. doi:10.1016/j.jhazmat.2019.121095

Li, S., Wang, F., Pan, W., Yang, X., Ni, J., Sun, W., et al. (2019). Molecular insights into the effects of Cu(II) on sulfamethoxazole and 17β-estradiol adsorption by carbon nanotubes/CoFe2O4 composites. *Chem. Eng. J.* 373, 995–1002. doi:10.1016/j.cej.2019.05.111

Li, Z., Li, M., Wang, Z., and Liu, X. (2020a). Coadsorption of Cu(II) and tylosin/sulfamethoxazole on biochar stabilized by nano-hydroxyapatite in aqueous environment. *Chem. Eng. J.* 381, 122785. doi:10.1016/j.cej.2019.122785

Liao, P., Li, B., Xie, L., Bai, X., Qiao, H., Li, Q., et al. (2020). Immobilization of Cr(VI) on engineered silicate nanoparticles: Microscopic mechanisms and site energy distribution. *J. Hazard. Mater.* 383, 121145. doi:10.1016/j.jhazmat.2019.121145

Liu, F.-F., Zhao, J., Wang, S., and Xing, B. (2016). Adsorption of sulfonamides on reduced graphene oxides as affected by pH and dissolved organic matter. *Environ. Pollut.* 210, 85–93. doi:10.1016/j.envpol.2015.11.053

Liu, H., Wei, Y., Luo, J., Li, T., Wang, D., Luo, S., et al. (2019). 3D hierarchical porous-structured biochar aerogel for rapid and efficient phenicol antibiotics removal from water. *Chem. Eng. J.* 368, 639–648. doi:10.1016/j.cej.2019.03.007

Liu, J., Zhou, D., Xu, Z., and Zheng, S. (2017). Adsorptive removal of pharmaceutical antibiotics from aqueous solution by porous covalent triazine frameworks. *Environ. Pollut.* 226, 379–384. doi:10.1016/j.envpol.2017.03.063

Liu, L., Cui, W., Lu, C., Zain, A., Qian, X., Shen, G., et al. (2020). Analyzing the adsorptive behavior of Amoxicillin on four Zr-MOFs nanoparticles: Functional groups dependence of adsorption performance and mechanisms. *J. Environ. Manag.* 268, 110630. doi:10.1016/j.jenvman.2020.110630

Liu, Q., Li, D., Cheng, H., Cheng, J., Du, K., Hu, Y., et al. (2021). High mesoporosity phosphorus-containing biochar fabricated from Camellia oleifera shells: Impressive tetracycline adsorption performance and promotion of pyrophosphate-like surface functional groups (C-O-P bond). *Bioresour. Technol.* 329, 124922. doi:10.1016/j.biortech.2021.124922

Liu, Y., Liu, X., Wang, H., Fang, Y., Li, Z., Lu, S., et al. (2022). Performance and mechanism of SMX removal in an electrolysis-integrated tidal flow constructed wetland at low temperature. *Chem. Eng. J.* 434, 134494. doi:10.1016/j.cej.2022.134494

Mimmo, T., Panzacchi, P., Baratieri, M., Davies, C. A., and Tonon, G. (2014). Effect of pyrolysis temperature on miscanthus (Miscanthus × giganteus) biochar physical, chemical and functional properties. *Biomass and Bioenergy* 62, 149–157. doi:10.1016/j.biombioe.2014.01.004

Nasuhoglu, D., Yargeau, V., and Berk, D. (2011). Photo-removal of sulfamethoxazole (SMX) by photolytic and photocatalytic processes in a batch reactor under UV-C radiation (λmax=254nm). *J. Hazard. Mater.* 186, 67–75. doi:10.1016/j.jhazmat.2010.10.080

Nielsen, L., Biggs, M. J., Skinner, W., and Bandosz, T. J. (2014). The effects of activated carbon surface features on the reactive adsorption of carbamazepine and sulfamethoxazole. *Carbon* 80, 419–432. doi:10.1016/j.carbon.2014.08.081

Pap, S., Taggart, M. A., Shearer, L., Li, Y., Turk, S. M. M., and Turk Sekulic, M. (2020). Removal behaviour of NSAIDs from wastewater using a P-functionalised microporous carbon. *Chemosphere* 264, 128439. doi:10.1016/j.chemosphere.2020.128439

Peiris, C., Gunatilake, S. R., Mlsna, T. E., Mohan, D., and Vithanage, M. (2017). Biochar based removal of antibiotic sulfonamides and tetracyclines in aquatic environments: A critical review. *Bioresour. Technol.* 246, 150–159. doi:10.1016/j.biortech.2017.07.150

Liao, P., Ismael, Z. M., Zhang, W., Yuan, S., Bao, J., Wang, K., et al. (2012). Adsorption of dyes from aqueous solutions by microwave modified bamboo charcoal, *Chem. Eng. J.*, 195-196, 339–346. doi:10.1016/j.cej.2012.04.092

Rodríguez-Martínez, C. E., Segura, E. G., Fall, C., and Colín-Cruz, A. (2019). *Removal of sulfamethoxazole in aqueous solution by two activated carbons from secondary sludge and biomass*. Desalination and Water Treatment.

Shen, X., Guo, X., Zhang, M., Tao, S., and Wang, X. (2015). Sorption Mechanisms of Organic Compounds by Carbonaceous Materials: Site Energy Distribution Consideration. *Environ. Sci. Technol.* 49, 4894–4902. doi:10.1021/es506034e

Shu-Rong, W., Qian, L., Zhong-Yang, L., Li-Hua, W., and Ke-Fa, C. (2006). Mechanism study of cellulose pyrolysis using thermogravimetric analysis coupled with infrared spectroscopy. *J. Zhejiang Univ.* 1, 413–419. doi:10.1007/s11708-007-0060-8

Song, J., Messele, S. A., Meng, L., Huang, Z., and Gamal El-Din, M. (2021). Adsorption of metals from oil sands process water (OSPW) under natural pH by sludge-based Biochar/Chitosan composite. *Water Res.* 194, 116930. doi:10.1016/j.watres.2021.116930

Tran, H. N., You, S. J., Hosseini-Bandegharaei, A., and Chao, H. P. (2017). Mistakes and inconsistencies regarding adsorption of contaminants from aqueous solutions: A critical review. *Water Res.* 120, 88–116. doi:10.1016/j.watres.2017.04.014

Vivas, E. L., and Cho, K. (2021). Efficient adsorptive removal of Cobalt(II) ions from water by dicalcium phosphate dihydrate. *J. Environ. Manag.* 283, 111990. doi:10.1016/j.jenvman.2021.111990

Wang, F. Y., Wang, H., and Ma, J. W. (2010). Adsorption of cadmium (II) ions from aqueous solution by a new low-cost adsorbent--bamboo charcoal. *J. Hazard. Mater.* 177, 300–306. doi:10.1016/j.jhazmat.2009.12.032

Wang, H., Yuan, X., Wu, Y., Chen, X., Leng, L., Wang, H., et al. (2015). Facile synthesis of polypyrrole decorated reduced graphene oxide–Fe3O4 magnetic composites and its application for the Cr(VI) removal. *Chem. Eng. J.* 262, 597–606. doi:10.1016/j.cej.2014.10.020

Wang, X., Shu, L., Wang, Y., Xu, B., Bai, Y., Tao, S., et al. (2011). Sorption of peat humic acids to multi-walled carbon nanotubes. *Environ. Sci. Technol.* 45, 9276–9283. doi:10.1021/es202258q

Wu, Q., Zhang, Y., Cui, M.-h., Liu, H., Liu, H., Zheng, Z., et al. (2022). Pyrolyzing pharmaceutical sludge to biochar as an efficient adsorbent for deep removal of fluoroquinolone antibiotics from pharmaceutical wastewater: Performance and mechanism. *J. Hazard. Mater.* 426, 127798. doi:10.1016/j.jhazmat.2021.127798

Xiong, Z.-H., Wang, L., Zhou, J.-G., and Liu, J.-M. (2010). Thermodynamics and kinetics of adsorption of diclofenac on magnetic multiwalled carbon nanotubes in an aqueous solution. *Acta Physico-Chimica Sin.* 26, 2890–2898. doi:10.3866/pku.whxb20101130

Yan, B., and Niu, C. H. (2018). Adsorption behavior of norfloxacin and site energy distribution based on the Dubinin-Astakhov isotherm. *Sci. Total Environ.* 631-632, 1525–1533. doi:10.1016/j.scitotenv.2018.03.119

Yan, B., Niu, C. H., and Wang, J. (2017). Analyses of Levofloxacin Adsorption on Pretreated Barley Straw with Respect to Temperature: Kinetics, π–π Electron-Donor–Acceptor Interaction and Site Energy Distribution. *Environ. Sci. Technol.* 51, 8048–8056. doi:10.1021/acs.est.7b00327

Yuan, H., Lu, T., Huang, H., Zhao, D., Kobayashi, N., and Chen, Y. (2015). Influence of pyrolysis temperature on physical and chemical properties of biochar made from sewage sludge. *J. Anal. Appl. Pyrolysis* 112, 284–289. doi:10.1016/j.jaap.2015.01.010

Yuan, H., Lu, T., Zhao, D., Huang, H., Noriyuki, K., and Chen, Y. (2013). Influence of temperature on product distribution and biochar properties by municipal sludge pyrolysis. *J. Material Cycles Waste Manag.* 15, 357–361. doi:10.1007/s10163-013-0126-9

Yuan, J. H., Xu, R. K., and Zhang, H. (2011). The forms of alkalis in the biochar produced from crop residues at different temperatures. *Bioresour. Technol.* 102, 3488–3497. doi:10.1016/j.biortech.2010.11.018

Zeng, S., and Kan, E. (2022). FeCl3-activated biochar catalyst for heterogeneous Fenton oxidation of antibiotic sulfamethoxazole in water. *Chemosphere* 306, 135554. doi:10.1016/j.chemosphere.2022.135554

Zhang, L., Niu, W., Sun, J., and Zhou, Q. (2020a). Efficient removal of Cr(VI) from water by the uniform fiber ball loaded with polypyrrole: Static adsorption, dynamic adsorption and mechanism studies. *Chemosphere* 248, 126102. doi:10.1016/j.chemosphere.2020.126102

Zhang, R., Zheng, X., Chen, B., Ma, J., Niu, X., Zhang, D., et al. (2020c). Enhanced adsorption of sulfamethoxazole from aqueous solution by Fe-impregnated graphited biochar. *J. Clean. Prod.* 256, 120662. doi:10.1016/j.jclepro.2020.120662

Zhang, T.-Y., Lu, Y.-S., Luo, Z.-N., Sun, W.-J., Xu, B., Hu, C.-Y., et al. (2022). Micropollutant removal and disinfection byproduct control by sequential peroxymonosulfate-UV treatment in water: A case study with sulfamethoxazole. *J. Environ. Sci.* 117, 141–150. doi:10.1016/j.jes.2022.03.046

Zhang, X., Chu, Y., Zhang, H., Hu, J., Wang, X., Wu, X., et al. (2021). A mechanistic study on removal efficiency of four antibiotics by animal and plant origin precursors-derived biochars. *Sci. Total Environ.* 772, 145468. doi:10.1016/j.scitotenv.2021.145468

Zhang, Y., Peng, D., Luo, Y., Huang, D., Guo, X., and Zhu, L. (2020b). Cellulase modified waste biomass to remove sulfamethazine from aqueous solutions. *Sci. Total Environ.* 731, 138806. doi:10.1016/j.scitotenv.2020.138806

Zhao, H., Liu, X., Cao, Z., Zhan, Y., Shi, X., Yang, Y., et al. (2016). Adsorption behavior and mechanism of chloramphenicols, sulfonamides, and non-antibiotic pharmaceuticals on multi-walled carbon nanotubes. *J. Hazard. Mater.* 310, 235–245. doi:10.1016/j.jhazmat.2016.02.045

Zhou, Y., Liu, X., Xiang, Y., Wang, P., Zhang, J., Zhang, F., et al. (2017). Modification of biochar derived from sawdust and its application in removal of tetracycline and copper from aqueous solution: Adsorption mechanism and modelling. *Bioresour. Technol.* 245, 266–273. doi:10.1016/j.biortech.2017.08.178